Electronic Supplementary Information

Deep eutectic solvent strategy to form defect-rich N, S, and O Tridoped carbon/Co$_9$S$_8$ hybrid materials for pH-universal hydrogen evolution reaction

Hongyu Mou,[a] Zhimin Xue,[b] Baolong Zhang,[a] Xue Lan,[a] Tiancheng Mu[a,*]

[a] *Department of Chemistry, Renmin University of China, 59 Zhongguancun Street, Beijing 100872, PR China. E-mail: tcmu@ruc.edu.cn*

[b] *College of Materials Science and Technology, Beijing Forestry University, Beijing 100083, China.*

Table of the contents

1. Experiment Section

2. Supplementary Figures and Discussion

3. Supplementary Tables

4. References

1. Experiment Section

Chemicals and Materials

The CoCl·6H$_2$O, thiourea, K$_2$HPO$_4$, KH$_2$PO$_4$, and KOH were purchased from Shanghai Macklin Biochemical Co., Ltd. The H$_2$SO$_4$ was Sinopharm Chemical Reagent Co., Ltd. The 20 % Pt/C and nafion were purchased from Alfa Aesar Co., Ltd. Above reagents were stored in desiccators.

Preparation of N, S, O triple-doped carbon/Co$_9$S$_8$ composites.

The N, S, O triple-doped carbon/Co$_9$S$_8$ (NSOC/CS) composites were prepared by a solution processing, followed by pyrolytic of deep eutectic solvents yield NSOC/CS composites. The detailed steps are as follows: First, 0.01 mol CoCl$_2$·6H$_2$O and 0.01 mol thiourea were mixed well and placed in an oil bath at 70 ℃, and stirred to form a uniform liquid. The liquid was then coated on a carbon cloth and placed in a tube furnace under nitrogen atmosphere at 550 ℃ and held for 4 hours. As the furnace cooled, the NSOC/CS composites were obtained. By changing the amount of thiourea in the experiment were 0.01mol, 0.02 mol, 0.04 mol for the preparation of NSOC/CS-1, NSOC/CS-2, NSOC/CS-3, respectively.

Electrochemical measurements.

HER polarization curve tests were conducted on a 3000 potentiostat/galvanostat with a three-electrode electrochemical cell. Graphite rod was used as the counter electrode and Ag/AgCl (saturated KCl filled) as the reference electrode. A carbon cloth electrode with an area of 1×1 cm^2 used as the working electrode. Experiments were conducted in an 0.5 M H$_2$SO$_4$, 1 M PBS (pH=7), and 1.0 M KOH electrolyte at room temperature. The potential range was from 0 to -1.5 V (vs. Ag/AgCl) and the scan rate was 5 mV·s^{-1}. Cyclic voltammetry (CV) was carried out to calculate the capacitance (C$_{dl}$), The obtained C$_{dl}$ can be converted into an electrochemically active surface area (ECSA) using the formula: ECSA $= \dfrac{C_{dl}}{C_s}$, where the specific capacitance value (C$_s$) was 40 μF·cm^{-2}.[1] All the polarization curves were recorded with a 80% iR compensation. As for the Faradaic efficiency measurements, gas chromatography (Agilent 6820, Ar carrier, molecule sieve 5A column, TCD detector) was used to determine the experimentally evolved amount of H$_2$. Faraday law to calculate the theoretical amount of H$_2$ expected based on a chronoamperometry.

Instrumentation and Characterization

Differential scanning calorimetry (DSC) was performed using a Q2000 DSC (TA Instruments-Waters LLC, USA) system at a heating rate of 10 °C·min^{-1}. XRD patterns were collected using a Rigaku D/max-2500 diffractometer. AFM was taken on a Bruker Multimode 8 instrument under the AC mode (tapping mode). Sample morphologies were characterized using a Hitachi SU8010 field emission scanning electron microscope (FESEM) and JEOL-2100F TEM. X-ray photoelectron spectroscopic (XPS) analysis was performed by an ESCALAB MK X-ray photoelectron spectrometer. The spectra were calibrated using the C1s (284.8 eV). We fit peaks by means of XPS-peak-differenating analysis software called "XPSPEAK4.0". FT-IR spectra were recorded on Bruker Tensor 27 IR spectrometer and the sample was prepared by the KBr pellet method. Specific surface areas and pore size distribution were analyzed on Micromeritics ASAP 2020 N_2 adsorption analyzer using the BET (Brunauer-Emmet-Teller) and BJH (Barrett-Joyner-Halenda) methods, respectively.

Density functional theory (DFT) calculation.

The present first principle DFT calculations are performed by Vienna Ab initio Simulation Package(VASP)[2] with the projector augmented wave (PAW) method.[3] The exchange-functional is treated using the generalized gradient approximation (GGA) of Perdew-Burke-Ernzerhof (PBE) functional.[4] The energy cutoff for the plane wave basis expansion was set to 450 eV and the force on each atom less than 0.02 eV/Å was set for convergence criterion of geometry relaxation. The Brillouin zone integration is performed using 2×5×1 k-point sampling. The self-consistent calculations apply a convergence energy threshold of 10^{-5} eV. The DFT-D3 method was employed to consider the van der Waals interaction.[5]
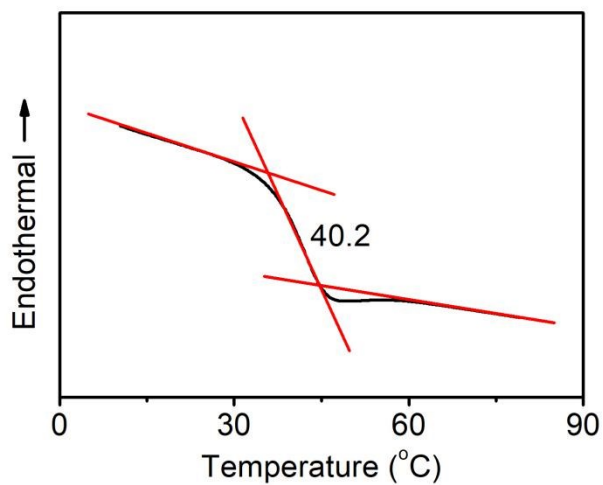
2. Supplementary Figures

Figure S1. DSC spectrum of DES ($CoCl_2 \cdot 6H_2O$ and thiourea mixture).

A Q2000 DSC (TA Instruments-Waters LLC, USA) system was applied to obtain differential scanning calorimetry (DSC) data with a heating rate of 10 °C·min^{-1}. DSC curves in Figure S1 proves that the $CoCl_2 \cdot 6H_2O$ and thiourea mixture starts to melt from 40.2 °C. This eutectic temperature is lower than the melting point of thiourea (171 °C) and $CoCl_2 \cdot 6H_2O$ (86 °C), which demonstrated the formation of homogenous liquid.
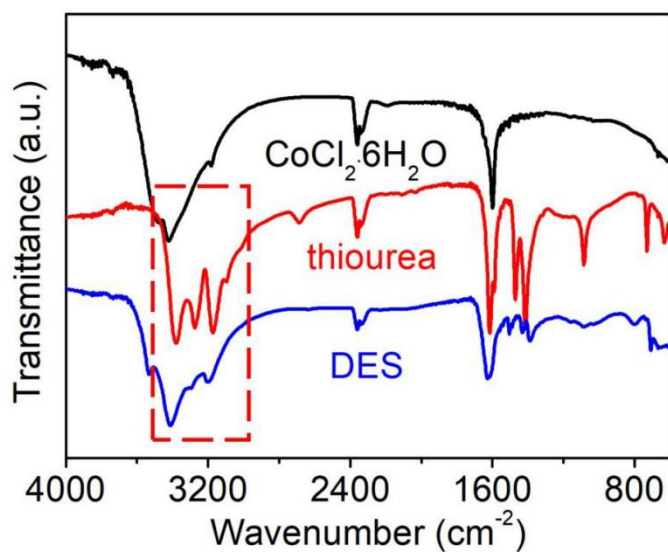
Figure S2. FT-IR spectra of $CoCl_2 \cdot 6H_2O$, thiourea, and DES ($CoCl_2 \cdot 6H_2O$ and thiourea mixture).

A Bruker Tensor 27 IR spectrometer was used to record FT-IR spectra. The samples for FT-IR spectra experiments were prepared by the KBr pellet method. It can be seen from the FTIR spectra that there is a clear N-H stretching vibration peak for thiourea at 3000~3600 cm^{-1}. After the solution is formed, the N-H stretching vibration peak basically disappears and the peak shape becomes dull, suggesting that the fine structure of urea has disappeared, suggesting that the fine structure of thiourea disappears, indicating that there is an interaction between $CoCl_2 \cdot 6H_2O$ and thiourea. All of the above interactions are contributed to the formation of homogeneous ionic liquid.
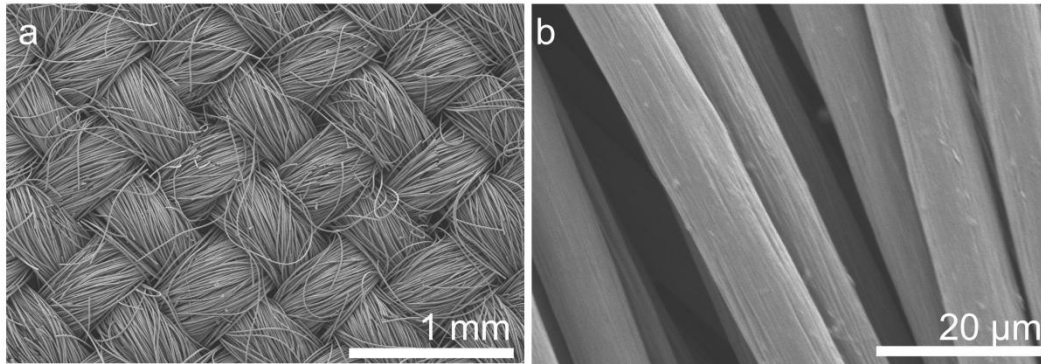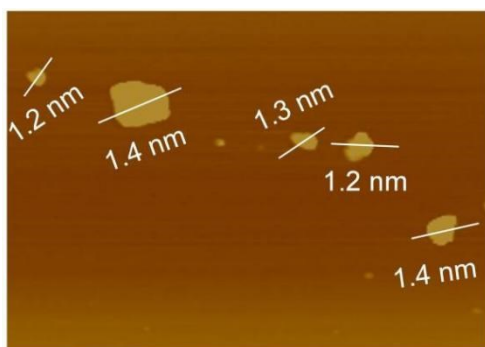
Figure S3. FESEM images of the bare CC.

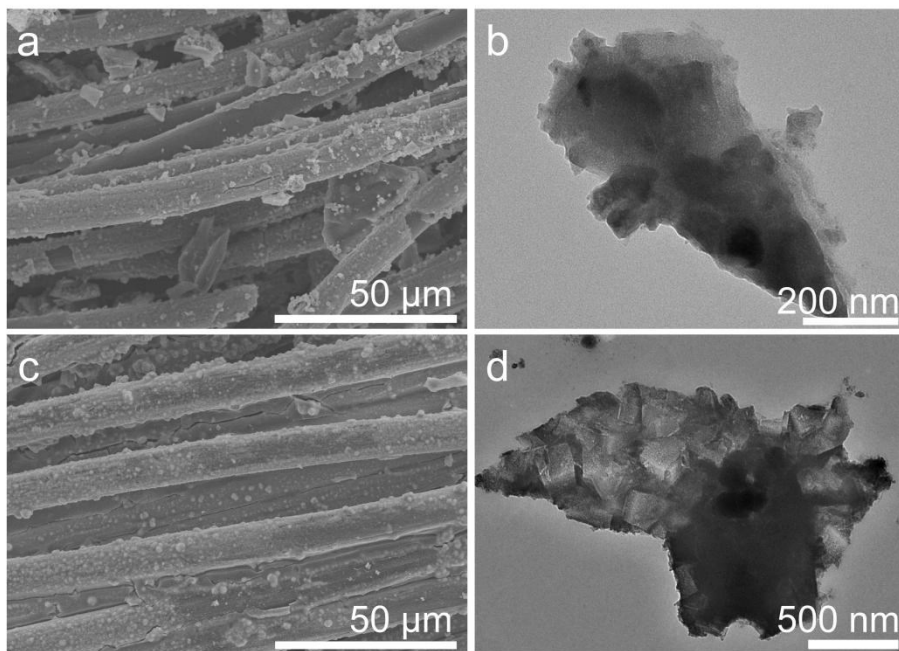**Figure S4.** AFM analysis of the NSOC/CS.

Figure S5. FESEM images of the (a) NSOC/CS-2 and (c) NSOC/CS-3, TEM images of the (b) NSOC/CS-2 and (d) NSOC/CS-3.

The morphologies of the synthesized samples with different $CoCl_2 \cdot 6H_2O$ and thiourea ratios were studied by FESEM and TEM, as shown in Figure S5. With the increase of thiourea content, the products generated in the carbon fiber shell agglomerate together (Figure S5a and c), and the thickness of the nanosheet increases (Figure S5b and d), which may be due to the increase of thiourea content and the increase of pyrolysis carbon content, resulting in the agglomerate of carbon.
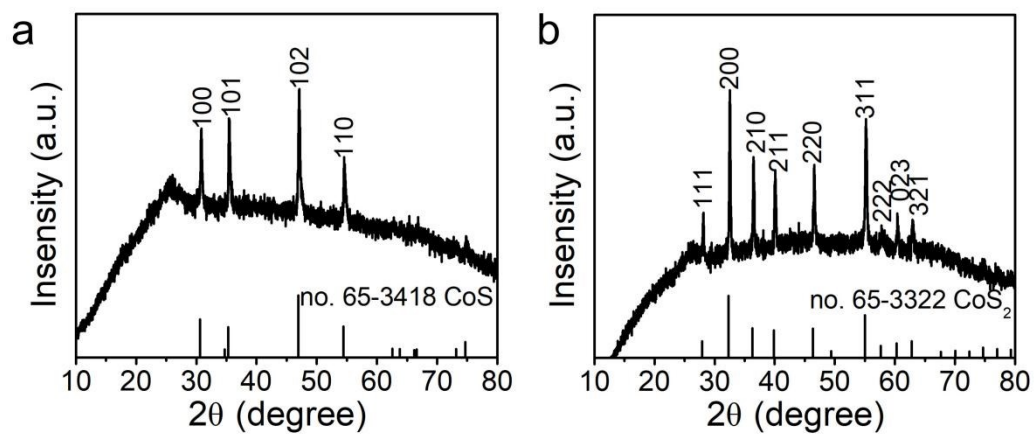

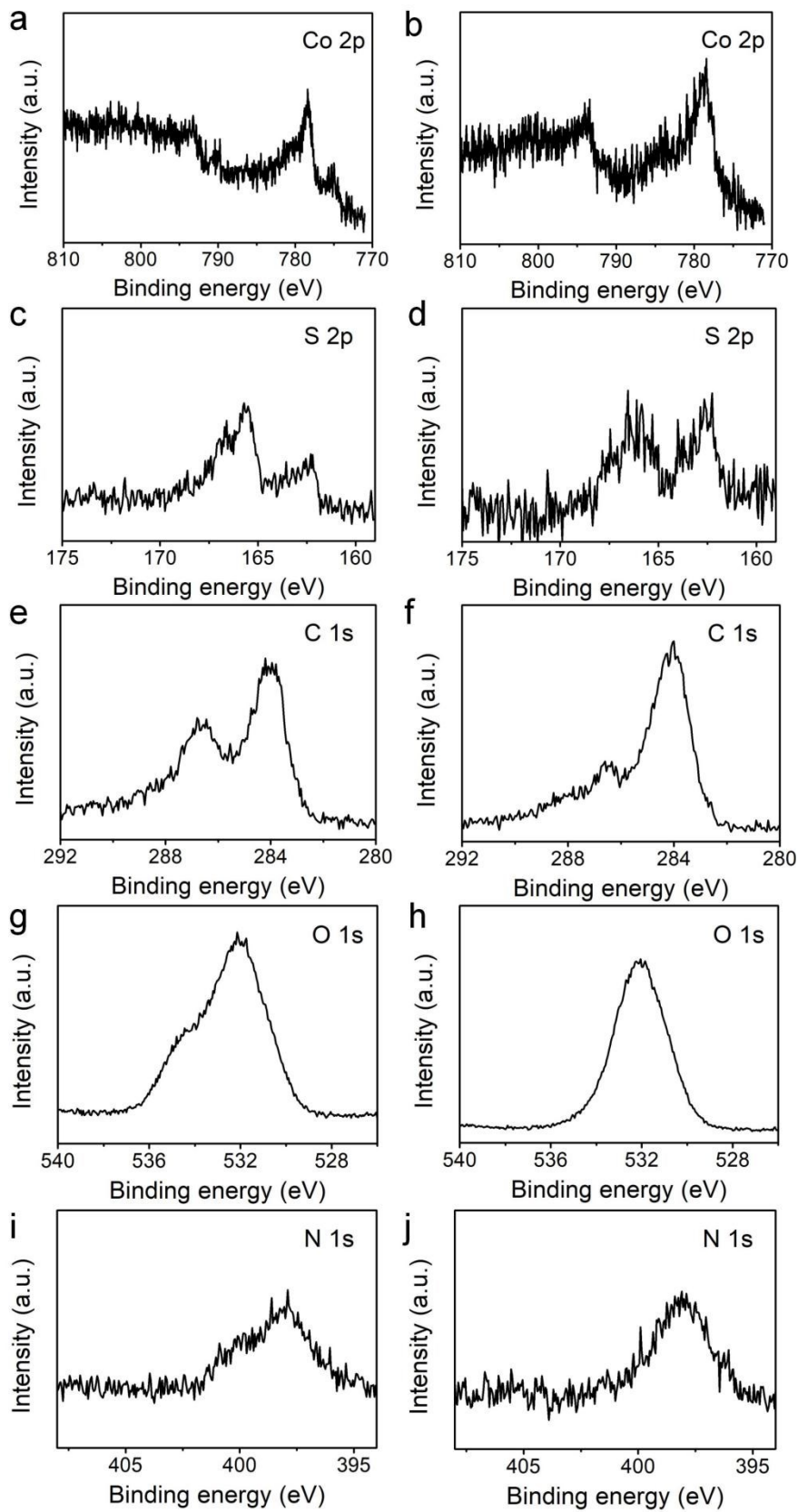**Figure S6.** XRD patterns of the a) NSOC/CS-2 and b) NSOC/CS-3.

Figure S7. Co 2p, S 2p, C 1s, O 1s, and N 1s high resolution XPS spectra of the a, c, e, j, i) NSOC/CS-2 and b, d, f, h, j) NSOC/CS-3.
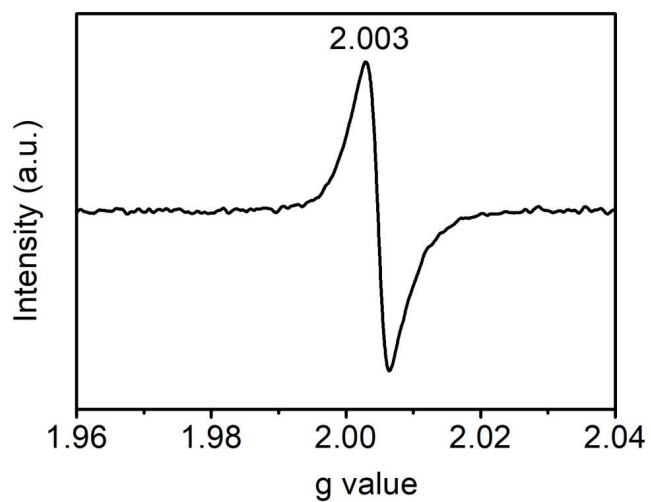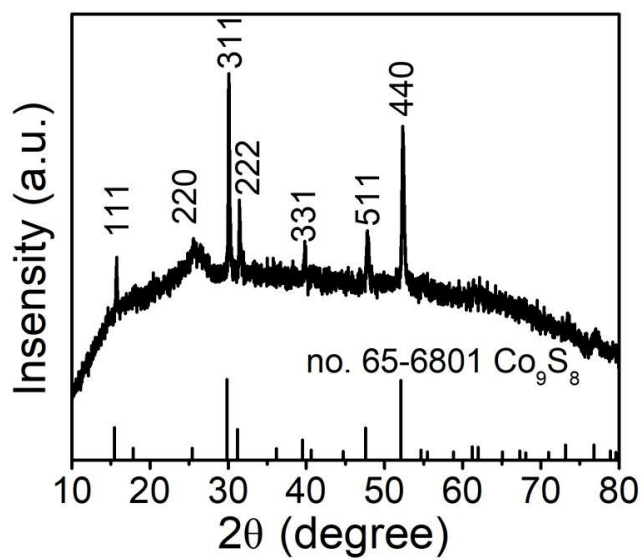
Figure S8. EPR spectrum of NSOC/CS-1.

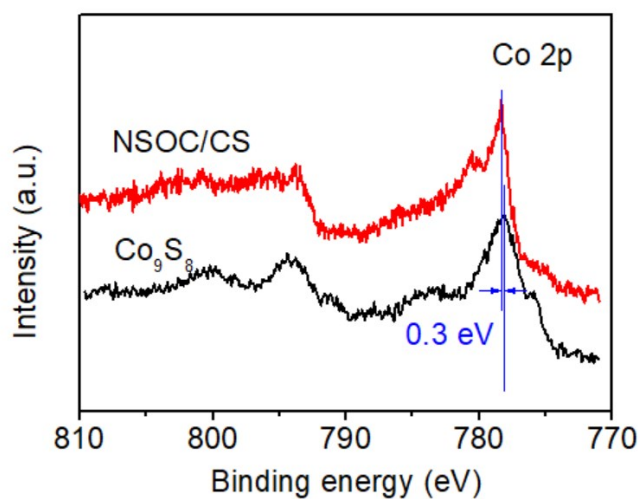**Figure S9.** XRD patterns of the NSOC/CS-1.

Figure S10. The Co 2p high-resolution XPS of Co_9S_8 and NSOC/CS spectra.
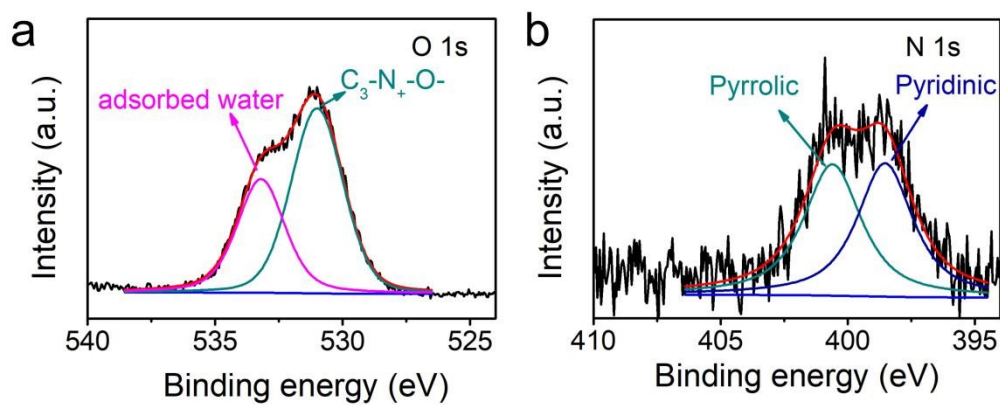

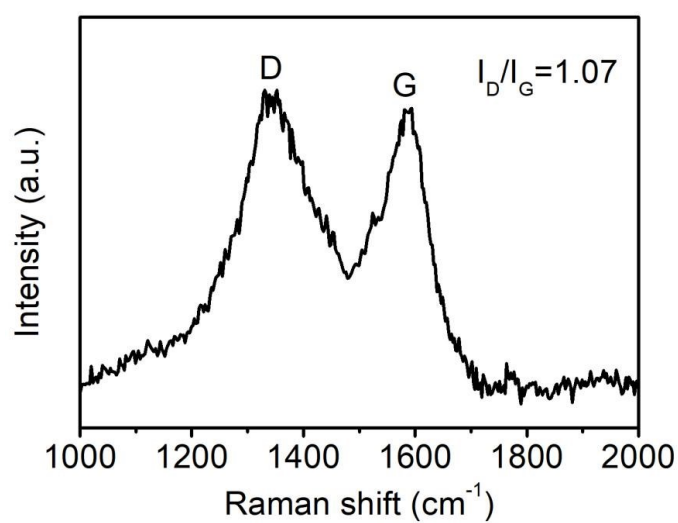**Figure S11.** The a) O 1s and b) N 1s high-resolution XPS of NSOC/CS spectra.

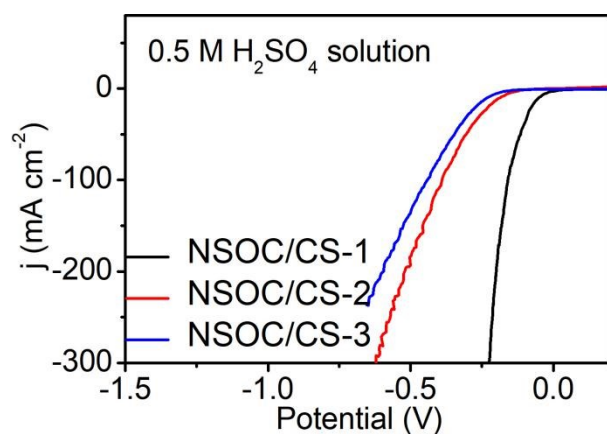**Figure S12.** Raman spectrum of NSOC/CS.

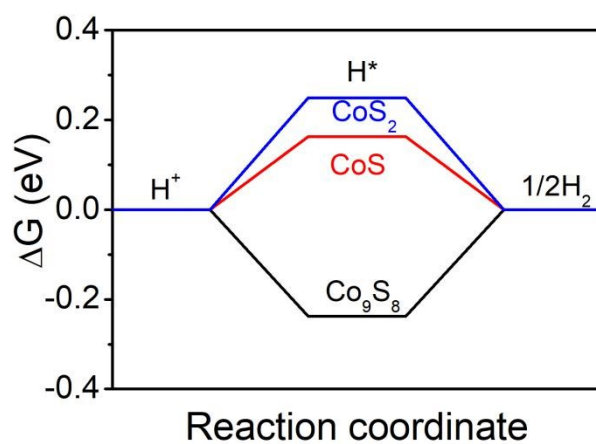**Figure S13.** LSV curves of NSOC/CS-1, NSOC/CS-2, and NSOC/CS-3.

Figure S14. Calculated free energy diagram of the HER on Co_9S_8, CoS, and CoS_2, respectively.
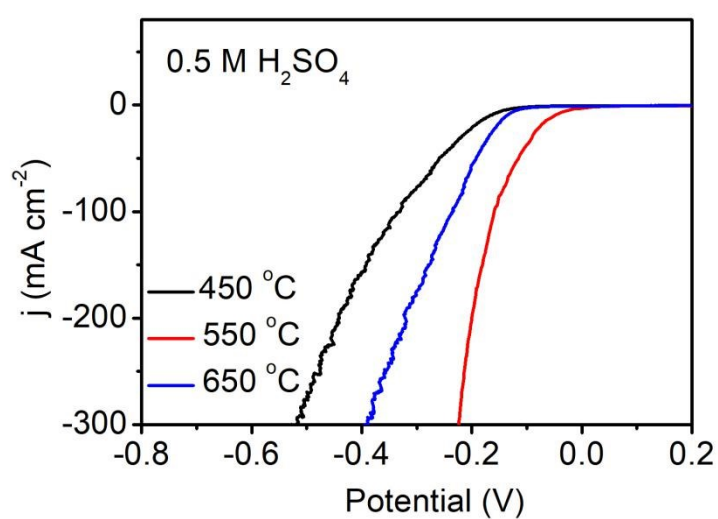

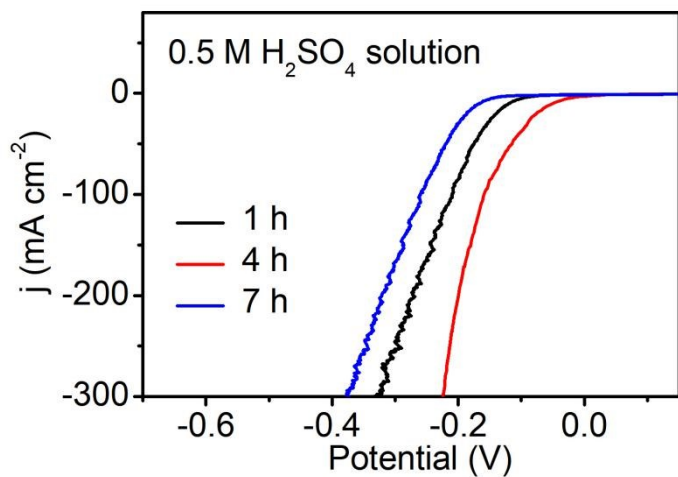**Figure S15.** LSV curves of NSOC/CS-450 °C, NSOC/CS-550 °C, and NSOC/CS-650 °C.

Figure S16. LSV curves of NSOC/CS-1 h, NSOC/CS-4 h, and NSOC/CS-7 h.
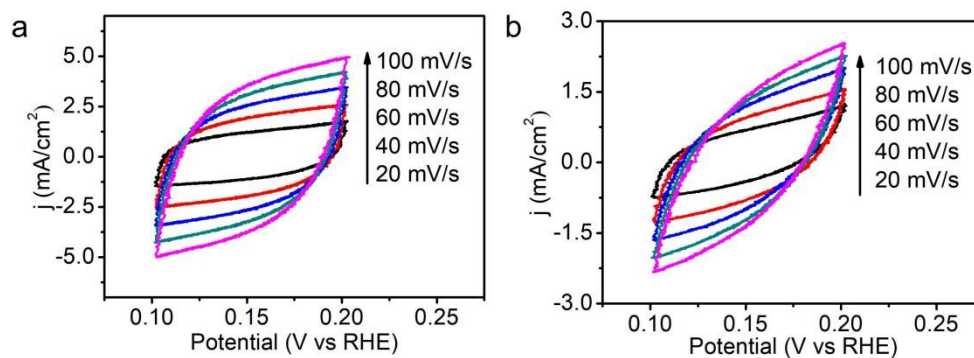
Figure S17. Cyclic voltammetry of NSOC/CS and Co_9S_8 (0.1-0.2 V vs. RHE) at different scan rate.
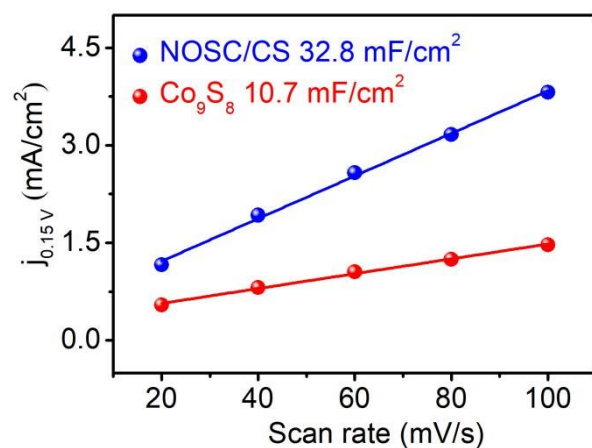
Figure S18. Differences in current density ($\Delta J = J_a - J_c$) against scan rates at 0.15 V vs RHE.
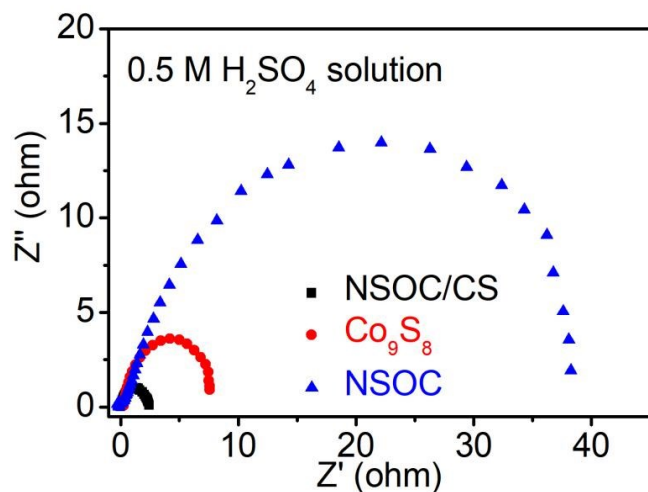
Figure S19. Nyquist plots of NSOC/CS, Co$_9$S$_8$, and NSOC.
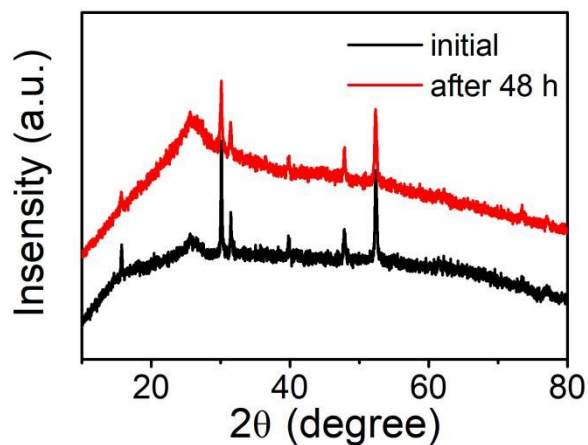
Figure S20. XRD patterns of initial and after stability experiments of NSOC/CS.
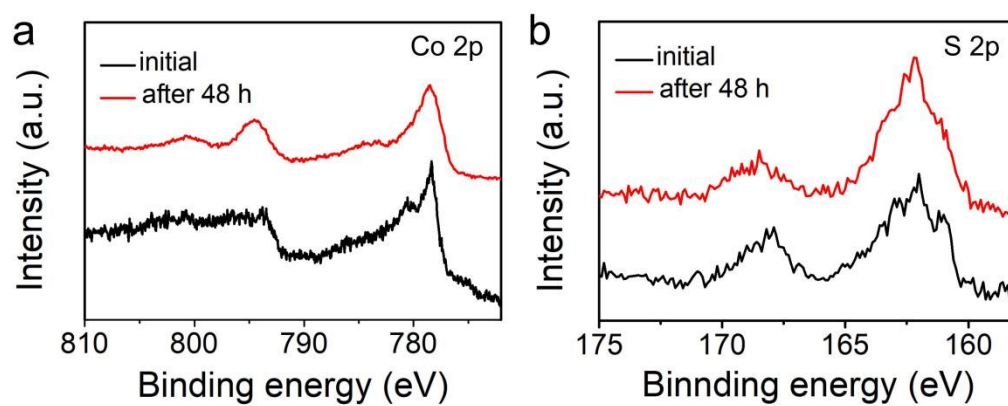
Figure S21. a) Co 2p and b) S 2p high resolution XPS spectra of the of NSOC/CS.
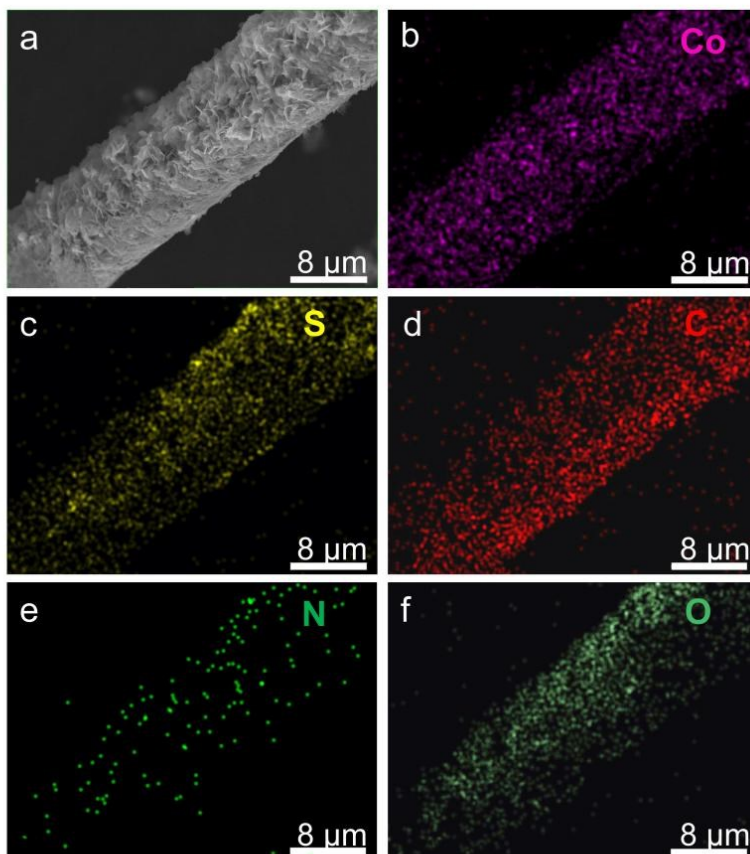
Figure S22. a) SEM image and b-f) elemental mapping of NSOC/CS after stability experiments.
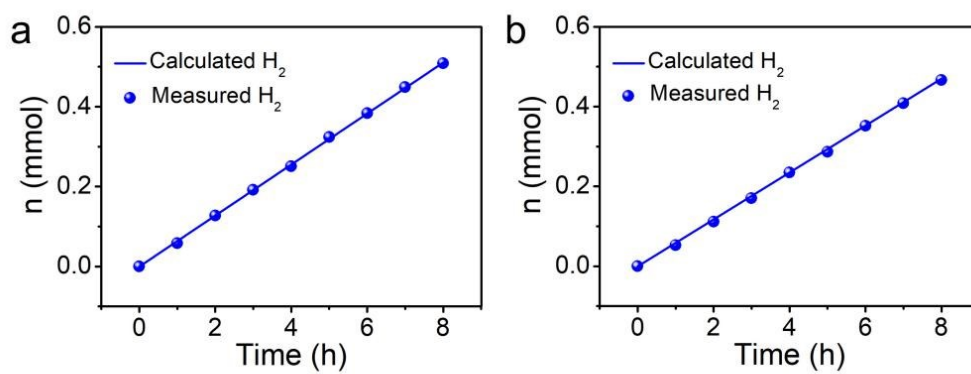
Figure S23. Amount of hydrogen theoretically calculated and experimentally measured versus time for NSOC/CS in 1 M a) KOH and b) PBS.
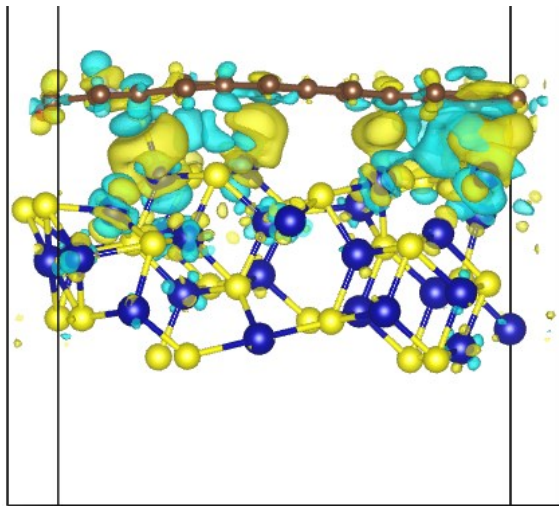
Figure S24. Differential charge density of NSOC/CS. Electrons depletion and electrons accumulation were displayed as blue and yellow isosurfaces, respectively.
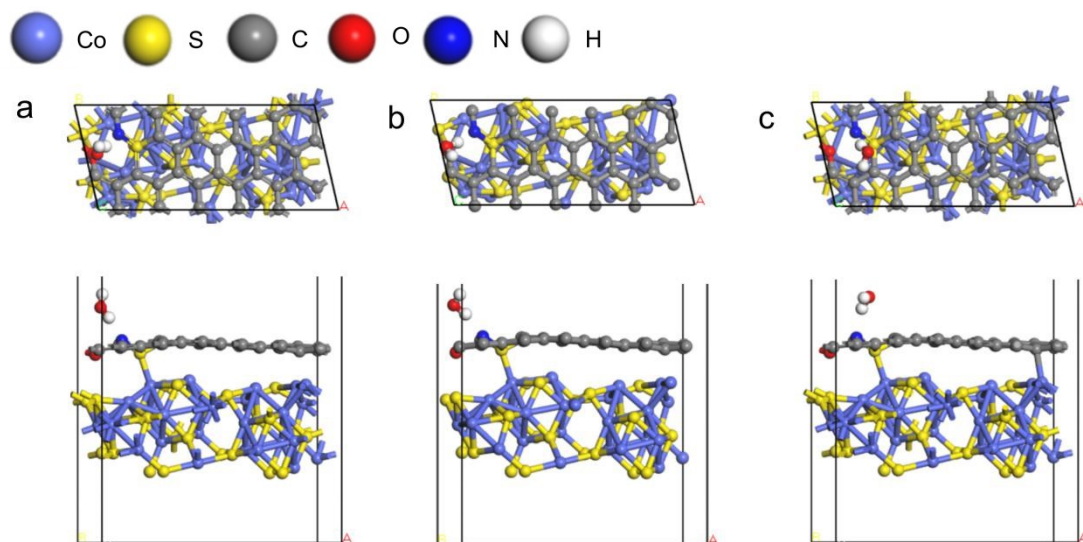
Figure S25. a) Adsorption structure diagram of H_2O molecules at N site, b) adsorption structure diagram of H_2O molecules at the O site (Optimized to migrate spontaneously to the N site), c) adsorption structure diagram of H_2O molecules at S site,
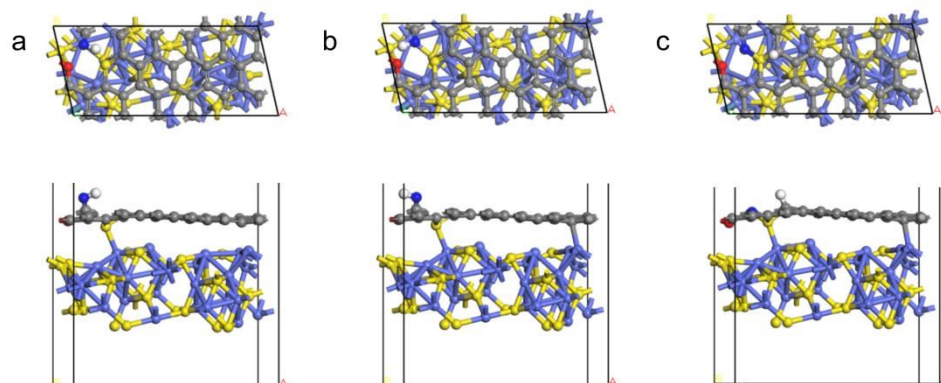
Figure S26. a) The adsorption structure of H$^+$ at the N site, b) the adsorption structure of H$^+$ at the O site (optimized to migrate spontaneously to the N site), c) the adsorption structure of H$^+$ at the S site.

3. Supplementary Tables

Table S1. Comparison of the relevant electrocatalysts for hydrogen evolution reation.

Catalysts	Electrolyte	η_{10} (mV)	Tafe Slope (mV dec^{-1})	Ref.
NSOC/CS	0.5 M H_2SO_4	53	45.3	this work
	1.0 M PBS	103	91.2	
	1.0 M KOH	68	31.0	
CoMoNiS-NF	0.5 M H_2SO_4	103	55	6
	1.0 M PBS	117	56	
	1.0 M KOH	113	85	
Co_9S_8/NC@MoS_2	0.5 M H_2SO_4	117	68.8	7
	1.0 M PBS	261	126.1	
	1.0 M KOH	67	60.3	
MxCo$_{3-x}$S$_4$	0.5 M H_2SO_4	80	47.5	8
	1.0 M PBS	90	-	
	1.0 M KOH	85	-	
CoNiP@NF	1.0 M KOH	155	115	9
	1.0 M Pi solution	120	103	
	0.5 M H_2SO_4	60	39	
Co_9S_8-MoS_2/NF	0.5 M H_2SO_4	-	79.58	10
	0.1 M PBS	152.1	99.4	
	1 M KOH	110	81.7	
Fe-(NiS_2/MoS_2)/CNT	1 M KOH	87	53	11
	0.5 M H_2SO_4	98	-	
	1 M PBS	127	-	

CoP HNS/CF	0.5 M H$_2$SO$_4$	48	57	
	0.5 M PBS	120	83	12
	1 M KOH	55	50	
Co$_{0.9}$S$_{0.58}$P$_{0.42}$	0.5 M H$_2$SO$_4$	139	88	13
	1 M KOH	141	72	
CoP	0.5 M H$_2$SO$_4$	160	56	14
	1 M KOH	175	84	
HI-CoP/CNT	1 M KOH	125	-	15
	0.5 M H$_2$SO$_4$	73	54.6	
meso-Fe-MoS$_2$/CoMo$_2$S$_4$	1 M KOH	122	90	16
O-CoP nanorods	1 M KOH	116	59	17
F–Ni$_3$S$_2$/NF	1 M KOH	38	78	18
Fe-Ni$_3$S$_2$/NF	1 M KOH	47	95	19
P-(Ni, Fe)$_3$S$_2$/NF	1 M KOH	98	88	20
NF-Ni$_3$S$_2$/MnO$_2$	1 M KOH	102	69	21
1D-CoS	1 M KOH	159	-	22
Fe-Ni$_2$P/MoS$_x$/NF	1 M KOH	112	76.6	23
S-CoO$_x$/NF	1 M KOH	136	80	24
S-CoSe$_2$	0.5 M H$_2$SO$_4$	88	50	25
Co-Co$_2$P@NPC/rGO	0.5 M H$_2$SO$_4$	61.5	51	26

4. References

(1) C. McCrory, S. Jung, J. C. Peters, T. F. Jaramillo, *J. Am. Chem. Soc.,* 2013, **135**, 16977–16987.

(2) G. Kresse, J. Furthmüller, *Comp. Mater. Sci.*, 1996, **6**, 15-50.

(3) P. E. Blöchl, *Phys. Rev. B*, 1994, **50**, 17953-17979.

(4) J. P. Perdew, J. A. Chevary, S. H. Vosko, K. A. Jackson, M. R. Pederson, D. J. Singh, C. Fiolhais, *Phys. Rev. B*, 1992, **46**, 6671-6687.

(5) S. Grimme, J. Antony, S. Ehrlich, H. Krieg, *J. Chem. Phys.,* 2010, **132**, 154104.

(6) Y. Yang, H. Yao, Z. Yu, S. M. Islam, H. He, M. Yuan, Y. Yue, K. Xu, W. Hao, G. Sun, H. Li, S. Ma, P. Zapol, M. G. Kanatzidis, *J. Am. Chem. Soc.,* 2019, **141**, 10417–10430.

(7) H. Li, X. Qian, C. Xu, S. Huang, C. Zhu, X. Jiang, L. Shao, L. Hou, *ACS Appl. Mater. Interfaces,* 2017, **9**, 28394–28405.

(8) Z. F. Huang, J. Song, K. Li, M. Tahir, Y. T. Wang, L. Pan, L. Wang, X. Zhang, J. J. Zou, *J. Am. Chem. Soc.,* 2016, **138**, 1359–1365.

(9) A. Han, H. Chen, H. Zhang, Z. Sun, P. Du, *J. Mater. Chem. A,* 2016, **4**, 10195–10202.

(10) M. Kim, M. A. R. Anjum, M. Choi, H. Y. Jeong, S. H. Choi, N. Park, J. S. Lee, *Adv. Funct. Mater.*, 2020, 2002536.

(11) C. Li, M. Liu, H. Ding, L. He, E. Wang, B. Wang, S. Fan, K. Liu, *J. Mater. Chem. A,* 2020, **8**, 17527–17536.

(12) H. Yoon, H. J. Song, B. Ju, D. W. Kim, *Nano Res.,* 2020, **13**, 2469–2477.

(13) Z. Dai, H. Geng, J. Wang, Y. Luo, B. Li, Y. Zong, J. Yang, Y. Q, *ACS Nano*, 2017, **11**, 11031–11040.

(14) A. Sumboja, T. An, H. Y. Goh, M. Luὶˆbke, D. P. Howard, Y. Xu, A. D. Handoko, Y. Zong, Z. Liu, *ACS Appl. Mater. Interfaces,* 2018, **10**, 15673–15680.

(15) A. Adam, M. H. Suliman, M. N. Siddiqui, Z. H. Yamani, B. Merzougui, M. Qamar, *ACS Appl. Mater. Interfaces,* 2018, **10**, 29407–29416.

(16) Y. Guo, J. Tang, J. Henzie, B. Jiang, W. Xia, T. Chen, Y. Bando, Y. M. Kang, M. S. A. Hossain, Y. Sugahara, Y. Yamauchi, *ACS nano*, 2020, **14**, 4141–4152.

(17) Y. Ma, G. Zhou, Z. Liu, L. Xu, D. Sun, Y. Tang, *Nanoscale,* 2020, **12**, 14733–14738.

(18) W. He, L. Han, Q. Hao, X. Zheng, Y. Li, J. Zhang, C. Liu, H. Liu, H. L. Xin, *ACS Energy Lett.,* 2019, **4**, 2905–2912.

(19) G. Zhang, Y. S. Feng, W. T. Lu, D. He, C. Y. Wang, Y. K. Li, X. Y. Wang, F. F. Cao, *ACS Catal.,* 2018, **8**, 5431–5441.

(20) C. Liu, D. Jia, Q. Hao, X. Zheng, Y. Li, C. Tang, H. Liu, J. Zhang, X. Zheng, *ACS Appl. Mater. Interfaces,* 2019, **11**, 27667–27676.

(21) Y. Xiong, L. Xu, C. Jin, Q. Sun, *Appl. Catal., B,* 2019, **254**, 329–338.

(22) S. A. Patil, I. Rabani, D. Vikraman, C. Bathula, N. K. Shrestha, H. Kim, S. Hussain, H. Im, *Int. J. Energy Res*., 2020, DOI: 10.1002/er.5973.

(23) X. Zhang, C. Liang, X. Qu, Y. Ren, J. Yin, W. Wang, W. Yang, W. Huang, X. Dong, *Adv. Mater. Interfaces,* 2020*, *1901926*.

(24) X. Yu, Z. Y. Yu, X. L. Zhang, P. Li, B. Sun, X. Gao, K. Yan, H. Liu, Y. Duan, M. R. Gao, G. Wang, S. H. Yu, *Nano Energy*, 2020, 104652.

(25) N. Xue, Z. Lin, P. Li, P. Diao, Q. Zhang, *ACS Appl. Mater. Interfaces,* 2020, **12**, 28288–28297.

(26) G. Li, J. Yu, J. Jia, L. Yang, L. Zhao, W. Zhou, H. Liu, *Adv. Funct. Mater.,* 2018, **28**, 1801332.